Spring 2023

The role of volatile enrichment in the radiogenic heating and thermal evolution of rocky exoplanets

Ula Jones

Asmaa Boujibar

Spring 2023

The role of volatile enrichment in the radiogenic heating and thermal evolution of rocky exoplanets

Ula Jones

The role of volatile enrichment in the radiogenic heating and thermal evolution of rocky exoplanets

Ula Jones, advised by Dr. Asmaa Boujibar

Abstract

Internal heating in terrestrial planets is a fundamental physical process controlling the internal structure of a planet, mantle convection, volcanic activity, and the generation of magnetic fields. Internal heating results from various processes including radioactive decay and accretional energy, as well as additional irradiation and tidal heating in planets with short orbital periods. The largest long-term heat source for terrestrial planets is radioactive heating, especially from the decay of uranium (U), thorium (Th), and potassium (K) isotopes. K is a moderately volatile element, while U and Th are refractory elements; during planetary accretion volatiles are depleted relative to refractory elements, but the extent of depletion from planet to planet depends on many factors including orbital radii and the rate of accretion during formation. Therefore, the amount of K present in a given body has significant implications for its thermal evolution. Through combining compositional trends observed in chondrites and planets with models of planetary differentiation and thermal evolution, we examine the role volatile depletion plays in radioactive heat generation and estimate the resulting amount of heat production. Additionally, we carry out heat flow calculations using the Virtual Planet Simulator (VPlanet) to relate radioactive heating to planetary thermal structure and compare our results to bulk planet heat flow.

Introduction

With the discoveries of over 5,000 confirmed exoplanets and counting, a small fraction of which are rocky, more and more information regarding their properties is becoming available. Observational data mainly allows exoplanetary mass and radius to be determined, though data regarding atmospheric compositions is slowly becoming more common. Only one exoplanetary magnetic field has been detected so far (Driscoll & Olson, 2011). Using knowledge of our own solar system planets, we can attempt to better understand exoplanet internal structures and geologic evolution. One topic we are particularly interested in is exoplanetary habitability, or the characteristics of exoplanets located in the habitable zone and likely to host atmospheres and liquid water.

Internal heating in terrestrial planets has significant implications for multiple planetary processes, including the development of tectonic regimes and magnetic field generation. This in turn can protect planetary surfaces from cosmic rays, as well as contribute to atmospheric development and maintenance. The most significant element of long-term planetary heat budgets is the heat generated by radioactive decay in planetary interiors. Therefore, radiogenic heating is a significant factor influencing planetary surface habitability, and the planetary composition inherited upon formation directly dictates the amount of energy generated by radionuclides in the interior (Lugaro et al, 2018). The heat generated by long lived radionuclides ^{232}Th, ^{235}U, ^{238}U, and ^{40}K contributes about 43% of Earth's long term heat budget (20 out of 46 TW), where the other half is mainly residual accretional heat from formation (Lay et al. 2008).

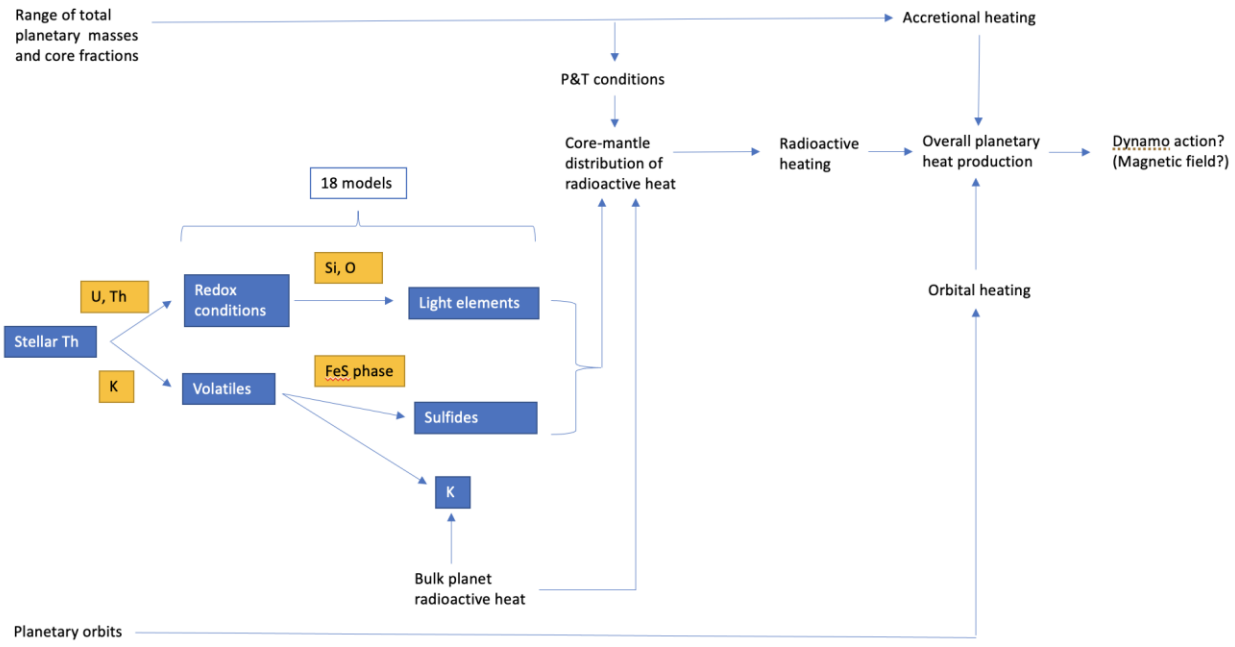

Figure 1. Overview figure describing how different geochemical and geophysical factors influence the distribution of and amount of internal heat over a planetary lifetime. The colored boxes indicate geochemical modeling specifically.

Magnetic field generation is a significant process to constrain when considering planetary habitability. A magnetosphere is defined as a massive magnetic field surrounding an astronomical body that often takes the form of a symmetric dipole for terrestrial planets. Intrinsic magnetic fields exist for half of the terrestrial planets in our solar system, or Earth and Mercury. Magnetic field deflection of charged solar particles can reduce rates of long-term atmospheric loss due to particle bombardment, which means the presence of a magnetosphere is often considered a prerequisite for habitability by astrobiologists and planetary scientists (Lugaro et al., 2018).

In order to generate an intrinsic magnetic field, the interior of a planet must be capable of maintaining geodynamo action over long periods of time. Therefore, it must contain a highly conductive, convective fluid. For terrestrial planets, this takes the form of molten iron in the outer core. The presence of insufficient internal heating can thereby prevent the formation of this fluid or the maintenance of sufficient convection within it.

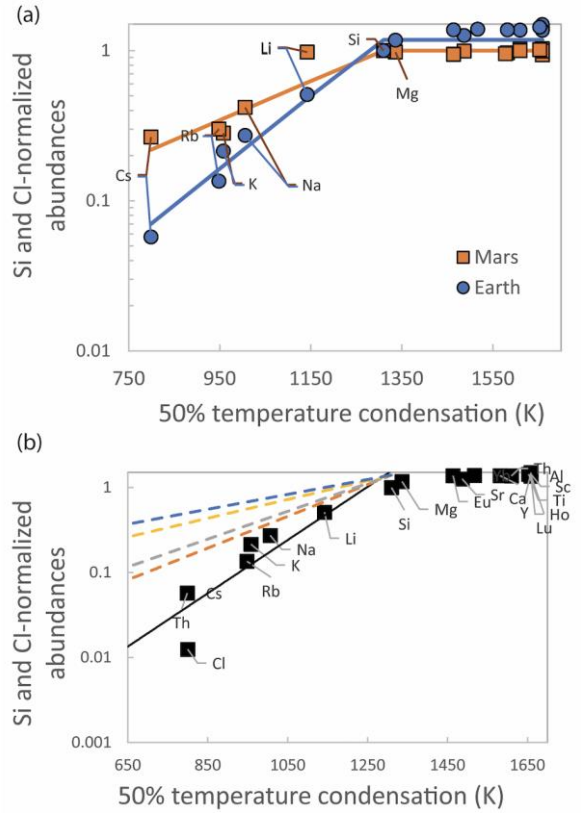

Figure 2: a) Plot comparing the mantle compositions of Mars and Earth (McDonough and Sun, 1995), as normalized to CI chondrites and Si concentration (Wasson and Kallemeyn, 1988), arranged by increasing 50% concentration temperature (K) (Lodders, 2003). The more volatile an element is, the more depleted it is in both planets, but Earth contains progressively less

volatile elements relative to Mars. b) Si and CI normalized elemental abundances in Earth's mantle arranged by increasing 50% concentration temperature (K). Colored dashed lines are modeled compositions for scenarios where the planet is more enriched in volatiles calculated following Boujibar et al. (2020) (see text for more details).

Several geochemical factors directly control the starting abundance of radiogenic elements in planetary interiors, one of which is volatile depletion. Our solar system specifically shows an increase with heliocentric distance in the abundance of elements that prefer the vapor phase. This trend explains the dichotomy between the compositions of planets located in the inner and outer solar system (Boujibar et al., 2020). The inner solar system contains terrestrial planets composed of iron cores and silicate mantles, while the outer region contains giant planets composed of ices and gasses. Volatile distribution between the inner and outer solar system directly accounts for this trend, as the outer planets are much more enriched in volatiles. There is a clear volatile depletion trend that exists in the inner solar system as well, which essentially mimics that of the solar system on a smaller scale (Figure 2). We also observe a clear decrease in the K/Th ratio between Venus, Earth, Mars and the asteroid Vesta (e.g. Boujibar et al. 2019). However, the existence of this trend in other solar systems is unknown, so we must address the effect of volatile content on the thermal evolution of planets in general.

This process directly affects the concentration of radiogenic elements present just after planetary formation due to potassium's status as a moderately volatile element. This project attempted to constrain the effects of volatile depletion on the radioactive heat that might be generated in a range of hypothetical exoplanets by examining two compositional cases: Earth and Mars-like exoplanets, or respectively volatile depleted and reduced, and volatile enriched and oxidized planets. After deriving these compositions, we apply the VPlanet Earth Interior module (Barnes et al .2020) to model basic thermal and magnetic evolutions for these two scenarios.

Data and Methods

1. Volatile depletion

The extent of volatile depletion was calculated using a model derived from observational constraints from volatile depletion trends observed in meteorites (Boujibar, 2020). Alkali abundances normalized to Si and CI compositions were calculated from an exponential trend based on their half condensation temperatures (Boujibar, 2020) (1-2). X_A represents alkali abundance, which is normalized to CI chondrite compositions and Si concentration; X_0 represents refractory element concentrations, which are again normalized to Si and CI concentrations. $T_{50K}{}^{0}$ is temperature corresponding to onset of volatile depletion, or 1464 and 1310 K for Earth and Mars respectively. We set a values to 0.015 and 0.003 to replicate Earth and Mars like conditions respectively, and use python scripts to calculate the resulting elemental abundances for each case.

$$b = [\ ln(\frac{X_0/X_{Si}}{X_0{}^{CI}/X_0{}^{CI}}) - ln(a)]/T^0{}_{50K} \quad (1)$$

$$\frac{X_A/X_{Si}}{X_A{}^{CI}/X_0{}^{CI}} = a * exp^{(b*T^A{}_{50K})} \quad (2)$$

2. Oxidation state

Absolute mantle compositions were calculated based on oxidation trends in the inner solar system. The terrestrial planets show increasing FeO concentrations in the mantle with increasing heliocentric distance, while core sizes decrease with distance from the Sun (e.g. Putrika et al., 2021). Therefore, the FeO/Fe ratio increases with distance from the Sun. We define α as a proxy to describe redox state (3), and thereby determine how much iron is present in the mantle as opposed to the core of a planet. We take α values of 0.27 and 0.54 for the Earth and Mars-like cases respectively (Putrika et al., 2021). From here, stoichiometry is used to calculate absolute mantle compositions for each scenario (3-7).

$$\alpha_{Fe} = \frac{Fe^{mantle}}{Fe^{total}} \quad (3)$$

$$\alpha_{Fe} = \frac{Fe^{mantle}}{f_{mantle}Fe^{mantle} + f_{core}Fe^{core}} \quad (4)$$

$$Fe_{total} = f_{mantle}Fe^{mantle} + f_{core}Fe^{core} \quad (5)$$

$$Fe_{total} = (\frac{Fe}{Si}) \times (\frac{Fe}{Si})_{CI} \times Si_{total} \quad (6)$$

$$Si_{total} = f_{mantle} \times Si_{mantle} \quad (7)$$

3. Radiogenic heat calculations

Radioactive decay and resulting heat production was modeled using the decay constant and heat production values (W/kg) for the four isotopes we considered (Table 1). At a given time step, the heat production was calculated as the heat production (HP) times radionuclide abundance (N(t)) at that time (8-9). N_0 is the starting abundance, and λ is the decay constant for each radionuclide.

$$N(t) = N_0 e^{-\lambda t} \quad (8)$$

$$Q^{rad}(t) = N(t) * HP \quad (9)$$

Table 1: Starting chondritic concentrations, decay constants, and heat production values in W/kg for ^{232}Th, ^{235}U, ^{238}U, and ^{40}K.

	Chondritic N0	λ (decay constants)	Heat Production (W/kg)
^{238}U	2.6e-08	1.55E-10	9.46E-5
^{235}U	8.2E-09	9.85E-10	5.7E-4
^{232}Th	4.8e-08	4.95E-11	2.64E-5
^{40}K	1.2e-06	5.55E-10	2.92E-5

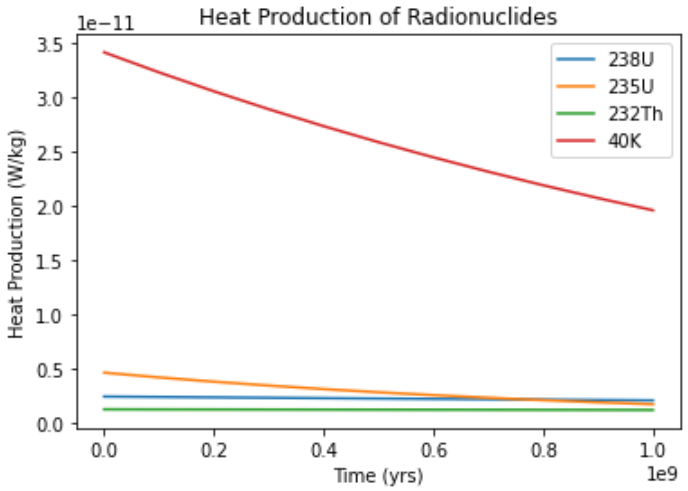

Figure 3. Heat production of long-lived radionuclides in W/Kg over a billion years after formation for a CI-like chondritic body with Earth-like nuclide abundances (^{40}K in red; note very large starting value).

4. VPlanet modeling

VPlanet is an open-source python simulation developed at the University of Washington that is capable of modeling many aspects of planetary evolution over billion year timescales (Barnes et al., 2020). The EarthInterior module uses models developed in Driscoll and Bercovici (2014) to estimate internal thermal structure and magnetic evolution over billions of years based on starting planetary characteristics, including radiogenic element abundances. Two ratios of Earth to Mars-like abundances of ^{232}Th, ^{235}U, ^{238}U, and ^{40}K radionuclides were derived from our calculations and used as input parameters relative to baseline Earth-like radionuclide abundances in the EarthInterior module.

Heat flow is derived directly from conservation of energy in the mantle, where Q_{surf} is the total surface heat loss and Q_{rad} represents the heat generated by radioactive decay (10). The thermal evolution equation is developed from conservation of energy and secular cooling in the mantle (11), where M_m is the mantle mass, and c_m is the specific heat (heat flow and thermal evolution for the core and CMB are developed similarly and coupled to mantle evolution

equations). Boundary layer depths at the upper mantle and lower mantle (δ_{UM} and δ_{LM}, repectively) are calculated over time based on the mantle viscosity (ν), the thermal boundary layer temperature jumps (ΔT), and the critical Rayleigh number for convection (Ra_c) (12-13), where α is the thermal expansivity and g is the surface gravity. Average upper and lower mantle kinematic viscosities are assumed to follow an Arrhenius law (14) where ν_0 is a reference viscosity, A_ν is activation energy, and R_g is the ideal gas constant. Inner core radius (R_{IC}) is determined by the intersection of the core adiabatic temperature profile with the iron solidus ($T_{Fe,0}$). R_{IC} can be derived as a function of D_N, the adiabatic length scale, the core Gruneisen parameter γ, and the iron solidus length scale D_{Fe}. Writing (15) as a function of core temperature and taking the time derivative gives the rate of inner core growth as a function of core cooling ($\dot{R_{ic}}$) (16), where T_c represents core temperature. Finally, the evolution of the magnetic moment (M), or essentially magnetic field strength, is estimated from the core energy balance and inner core growth rate using a scaling law (17). γ_d is the saturation constant for fast rotating dipolar dynamos, μ_0 is the magnetic permeability, $D_C = R_C - R_{IC}$ is the dynamo region shell thickness, and F_C is the core buoyancy flux (17).

$$Q_{surf} = Q_{conv} + Q_{melt} = Q_{rad} + Q_{CMB} + Q_{man} \quad (10)$$

$$\dot{T} = (Q_{rad} + Q_{CMB} - Q_{conv} - Q_{melt})/M_m c_m \quad (11)$$

$$\delta_{UM} = (Ra_c \frac{\nu_{UM}\kappa}{\alpha g \Delta T_{UM}})^{1/3} \quad (12)$$

$$\delta_{LM} = (Ra_c \frac{\nu_{LM}\kappa}{\alpha g \Delta T_{LM}})^{1/3} \quad (13)$$

$$\nu_{LM}(T) = \nu_0 exp[\frac{A_\nu}{R_g T_m}] \quad (14)$$

$$R_{ic} = R_c \sqrt{\frac{(D_N/R_c)^2 ln(T_{Fe,0}/T_{CMB}) - 1}{2(1-1/3\gamma_c)(D_N/D_{Fe})^2 - 1}} \quad (15)$$

$$\dot{R_{ic}} = -\frac{D^2{}_N}{2R_{ic}(2(1-1/3\gamma_c)(D_N/D_{Fe})^2 - 1)} \frac{\dot{T}_c}{T_c} \quad (16)$$

$$M = 4\pi R^3{}_c \gamma_d \sqrt{\rho/2\mu_0} (F_c D_c)^{1/3} \quad (17)$$

Results

1. Compositional modeling

Figure 4 shows results for our model of planetary mantle compositions normalized to Si and CI chondrites, calculated using equations (1) to (7) (see above). These compositions follow the exponential trend for the volatile elements and a constant value close to 1 for the refractory elements. As expected, we find a significantly higher concentration of K in the volatile-rich Mars-like compositional case, but higher refractory element concentrations (U, Th) for the Earth-like case (Figure 5). This is a product of the normalization, as decreasing the amount of volatile elements increases the relative amount of refractory elements. We calculate the starting amount of each isotope from isotopic abundances for ^{232}Th, ^{235}U, ^{238}U, and ^{40}K radionuclides (Table 2), using their natural abundances (Table 1).

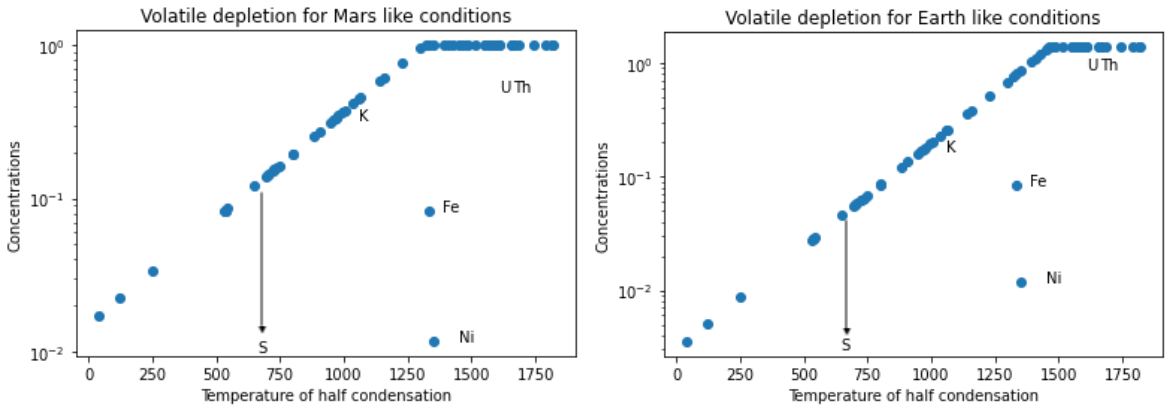

Figure 4: Mantle compositions for Earth and Mars-like compositional cases (respectively volatile depleted and reduced, and volatile enriched and oxidized). These compositions are normalized to Si abundance and CI chondrites (see equation 2). Iron, nickel, and sulfur are depleted in the mantles, where the extent of depletion is calculated using oxidation states. The Mars-like case is significantly more enriched in potassium.

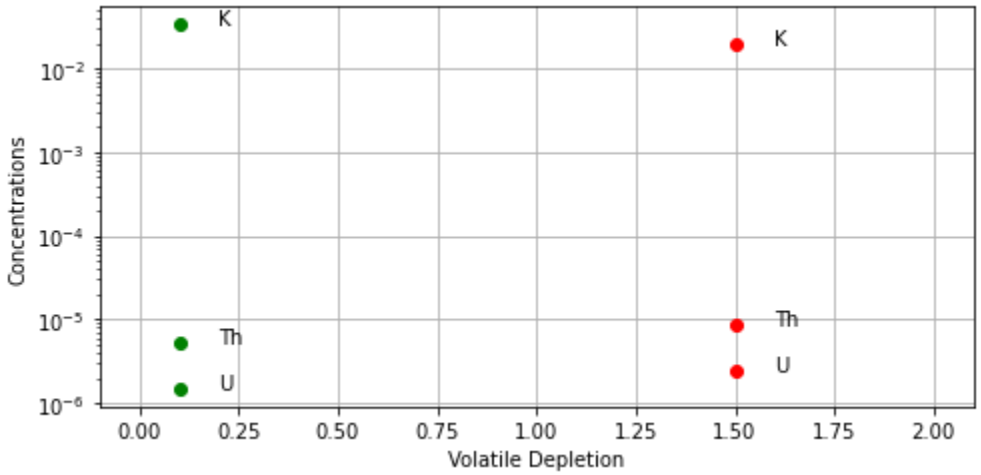

Figure 5: Dot plot showing concentrations of U, Th, and K between the Earth and Mars-like compositional cases. The Mars-like case is shown in green, and the Earth-like case in red. Changes in the relative concentrations of refractory elements U and Th are due to differences in normalization.

Table 2: Starting isotopic abundances for ^{232}Th, ^{235}U, ^{238}U, and ^{40}K for each compositional case,

	^{232}Th	^{235}U	^{238}U	^{40}K
Earth-like	8.46e-06	5.75e-07	1.82e-06	2.95e-05
Mars-like	5.30e-06	3.60e-07	1.14e-06	4.97e-05

2. Radioactive heat budgeting

We find significantly higher radioactive heat production for the Mars-like compositional case due to a higher starting concentration of ^{40}K (Figure 6). The heat produced by ^{232}Th, ^{235}U, and ^{238}U is lower at first, but maintains a more constant rate over billions of years. ^{235}U starts off higher than ^{232}Th and ^{235}U, but decreases at a faster rate.

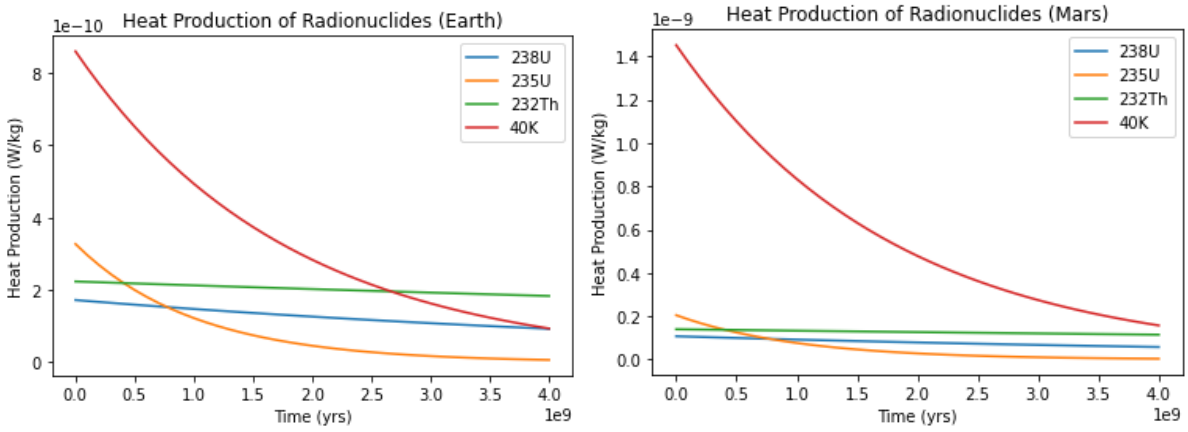

Figure 6: Rates of heat production over 4 billion years for ^{232}Th, ^{235}U, ^{238}U, and ^{40}K radionuclides for Earth-like and Mars-like cases. Note difference in y-axis scales, and higher radiogenic heat production for the Mars-like or volatile enriched case (especially for ^{40}K).

3. VPlanet Modeling

For both compositional cases, temperature decreases with planetary age, as does heat flow in each layer. Both boundary layer depths increase as temperature decreases and generally scale with viscosity in the upper and lower mantle. Results show slightly higher temperatures in Mars' core and CMB up to 2 billion years after formation, significantly higher CMB and core heat flows for this case, and slightly shallower boundary layer depths. Viscosity is very high just after crystallization for both cases, after which it increases linearly; however, the Mars-like model is slightly less viscous in both the upper and lower mantle due to higher temperatures generally for this case.

For the Earth-like model, inner core crystallization begins at around 4 billion years (Figure 7), which corresponds with the rapid increase in the magnetic moment at the same time. However, for the Mars-like case, inner core crystallization never occurs, due to the higher levels

of radiogenic heat derived from volatile enrichment causing its core and CMB temperatures to remain too high for any solidification. The magnetic moment therefore steadily decreases (Figure 8).

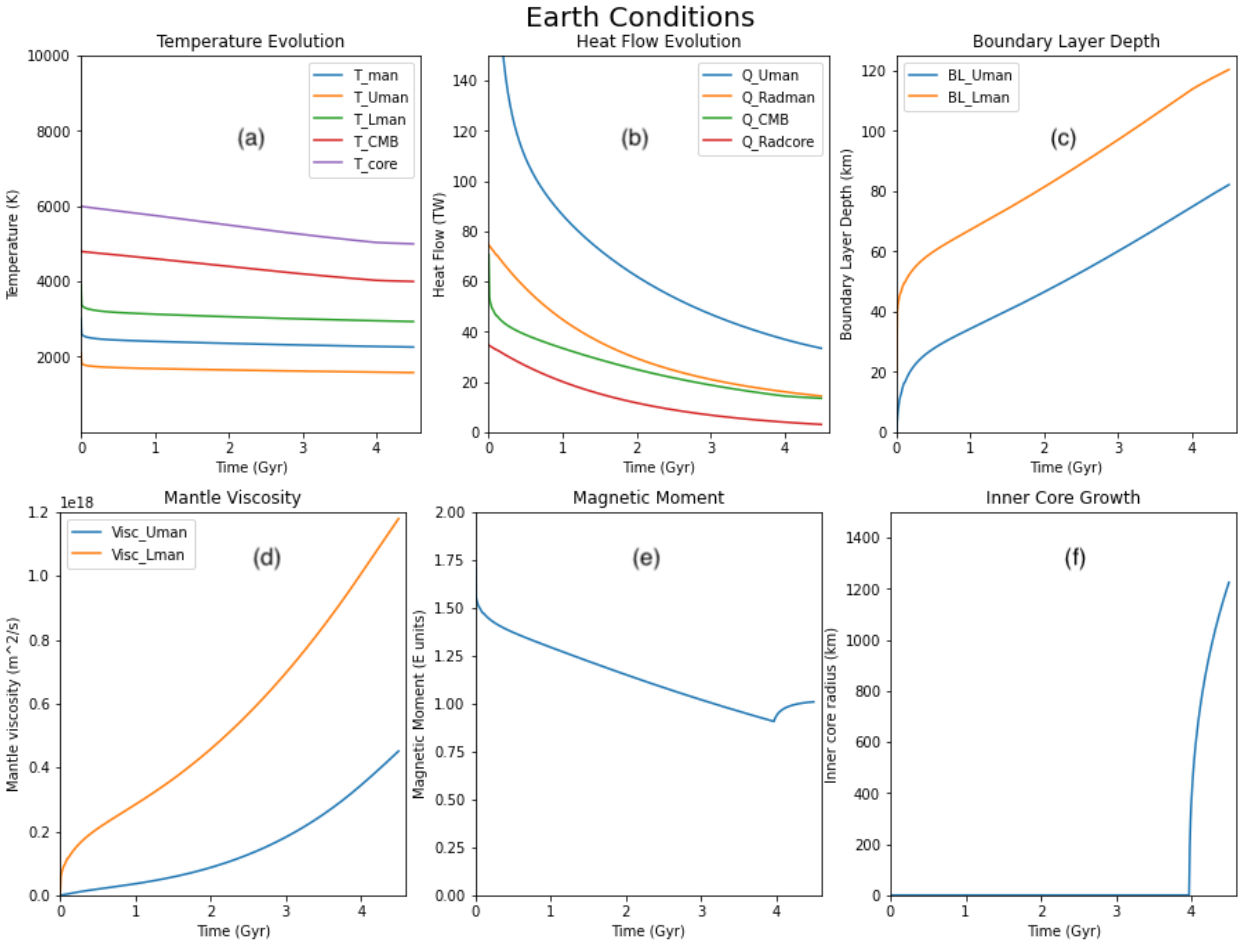

Figure 7: VPlanet (Barnes et al. 2020) output for thermal evolution, heat flow evolution, and boundary layer depths, mantle viscosity, magnetic moment, and inner core evolution for the VPlanet default earth-like starting composition. a) T_{man} = mantle temperature, T_{Uman} = upper mantle temperature, T_{Lman} = lower mantle temperature, T_CMB = core mantle boundary temperature, and T_core = core temperature. b) Q_{Uman} = total mantle heat flow, Q_{Radman} = mantle radioactive heating, Q_{CMB} = core mantle boundary heat flow, and $Q_{Radcore}$ = core radioactive heating. c) BL_{Uman} = mantle-surface boundary layer depth, BL_{Lman} = mantle-core boundary layer depth. d) $Visc_{Uman}$ = upper mantle viscosity, $Visc_{Lman}$ = lower mantle viscosity.

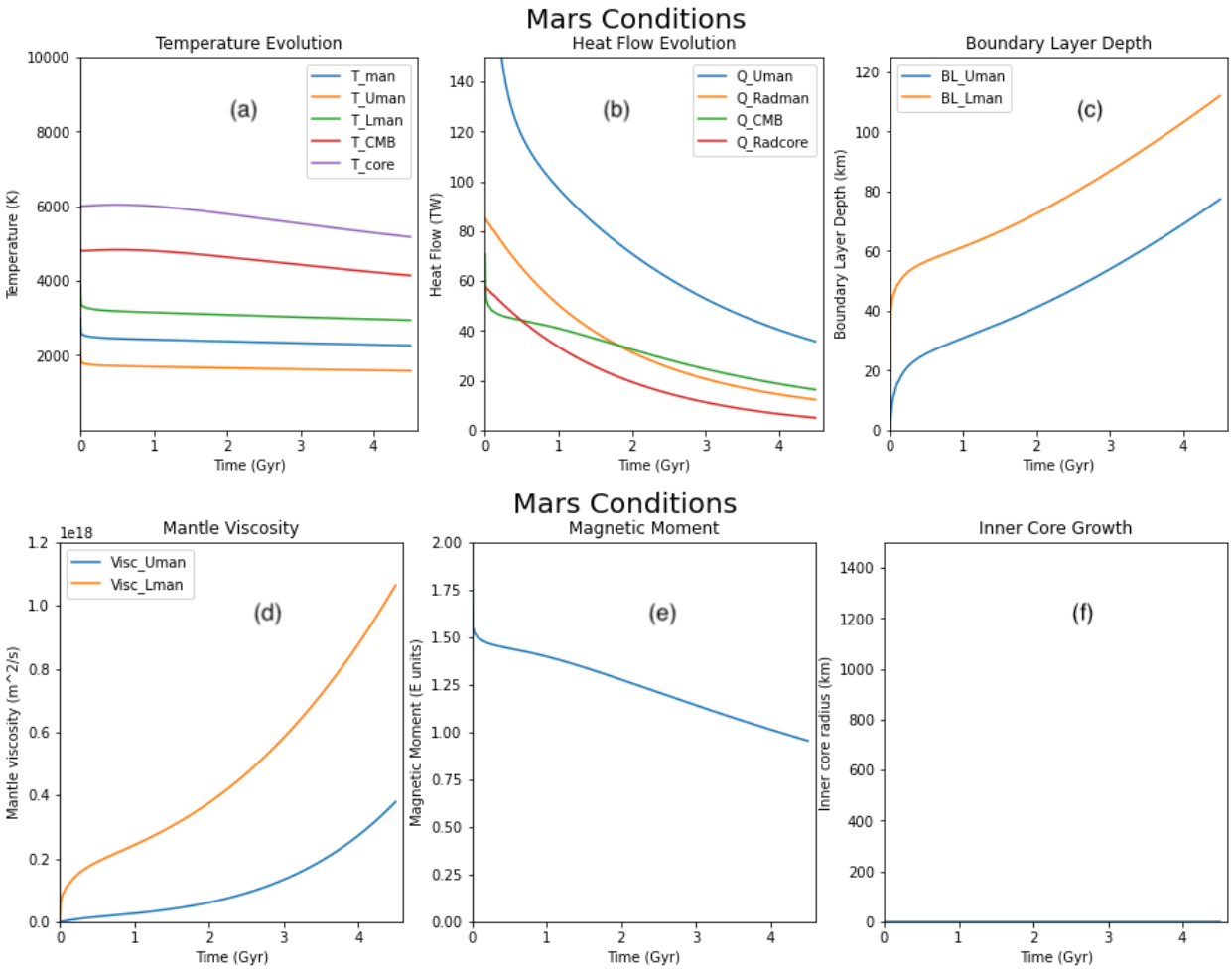

Figure 8: VPlanet (Barnes et al., 2020) output for thermal evolution, heat flow evolution, and boundary layer depths, mantle viscosity, magnetic moment, and inner core evolution, using the ratio between the Mars-like and Earth-like compositional cases as input parameters for U, Th, and K in the core, crust, and mantle.

Discussion

1. Mars' thermal evolution

While insufficient planetary heat, or too low of a core-mantle boundary temperature, can result in a solid core and thereby prevent magnetic field formation, the presence of too much heat can result in a fully liquid core, which also may have insufficient convection to generate a magnetic field (Boujibar et al., 2020). The ideal conditions for dynamo action are those intermediate pressure-temperature states for which inner core crystallization occurs. During this process, the release of light elements due to preferential partitioning into the liquid phase can enhance convection due to their upwards or downwards motion through the liquid outer core and the density gradient this creates, which can thereby help maintain dynamo action (Hemingway and Driscoll, 2021).

Our VPlanet results for the Mars-like compositional case are in agreement with the magnetic and thermal evolution of Mars itself, though we replicated its interior evolution from a perspective of volatile enrichment alone as opposed to other compositional trends that have likely played significant roles in its evolution. Indeed, Mars is known to have a core rich in light elements, including ~9 wt% S (Khan et al. 2020). The presence of significant S in Fe alloys has important implications for core evolution, including the decrease of its melting temperature (Morard et al. 2014). Hence, sulfur enrichment of Mars' core prolongs its liquid state, and this process likely constitutes the main reason for the absence of a geodynamo in Mars. In our model, we did not consider this enrichment of light elements of the core. Though, our Mars-like planets are assumed to have the same abundances of light elements as our Earth-like planets, inner core crystallization still never occurs due to the higher levels of radiogenic heat derived from volatile enrichment causing core and CMB temperatures to remain too high for any solidification, leading to a continual decline in the magnetic moment. Therefore, on a very simple level, we were able to replicate some aspects of the thermal and magnetic evolution of Mars based primarily on its radioactive heat budget, or level of volatile enrichment, as opposed to any other factors (such as the presence of light elements).

2. Future work
    1. The effects of sulfides on radiogenic element partitioning

One more significant geochemical trend that could be modeled and integrated into our heat budget calculations is the effect of sulfides on radiogenic element partitioning. Rocky planets that have large abundances of sulfur can include a sulfide phase in addition to the silicate and metallic phases. This process is due to the immiscibility of sulfides and Fe-rich alloys in multi-component systems (Boujibar et al. 2020). Element partitioning during planetary differentiation can be experimentally characterized and described using partitioning coefficients, or the amount of a given element present in a metal or sulfide phase divided by the silicate phase. Previous work showed that significant U, Th and K can partition into sulfides (Boujibar et al. 2019). Sulfide phases (e.g. FeS) are preferentially sequestered in planetary cores, meaning these phases can carry radiogenic elements into the core and trap heat there. Sulfide partitioning is influenced by light elements in the core and oxidation state as well, so this should also be considered in any application of partitioning; for instance, we could examine the role of sulfides in partitioning of radiogenic elements for oxidized and reduced compositions (see Figure 1). These results could then be combined with the modeling for radioactive heat generation previously described.

    2. Planetary masses

There is a massive range of exo-planetary sizes and compositions for which we could examine heat production, assuming an understanding of how material properties and planetary internal structures change with increasing temperature and pressure. Thermal budgeting that includes radiogenic heat contributions for massive rocky Super Earth exoplanets could be modeled as well (Boujibar et al., 2020).

3. Stellar compositions, tidal heating and radiative heating

Other significant factors that affect planetary heat budgets include stellar irradiation, tidal heating, and variations in the initial amounts of refractory radioactive elements from star to star. Studies have shown significant variations in stellar abundances of Th, with some stars exceeding 251% solar levels (Unterborn, 2015), which can significantly alter the internal heating that exoplanets experience based on stellar compositions alone. The composition of stars in different stellar neighborhoods is influenced by the chemical history of the galaxy as a whole, or galactic chemical evolution (GCE) trends. These models are used to better understand the formation, destruction and distribution of elements as they cycle through gas and stars over time (Bedell, 2018). Often, elemental abundances change as functions of stellar age.

Tidal heating and stellar irradiation can be significant factors in the heat budgets of planets with small orbital radii. The former is derived from friction resulting from differential gravitational forces exerted on a body as it orbits its center of mass. For example, the moon Io experiences extreme tidal forces as Jupiter's closest satellite; the heat generated by the dissipation of this energy in its crust results in a uniquely high degree of geologic activity. Radiative heating is simply the heat derived from stellar irradiation of planetary surfaces, and is mainly experienced by planets that orbit very close to their host stars.

Conclusions

We modeled the abundance of radioactive isotopes of rocky planets with varying abundances of volatiles and redox states, and showed K abundance is higher for volatile-rich planets like Mars. Therefore, these planets produce much higher radiogenic heat than volatile-depleted planets. Using these results, we then derived two planetary thermal evolution models for the two types of planets using the EarthInterior module of VPlanet simulation (Barnes et al. 2020). We found that the interior of Mars-like planets is hotter than Earth-like planets, preventing any crystallization of the iron core over 4.5 billion years. Therefore, Mars-like planets are unlikely to develop a self-sustaining magnetic field like Earth-like planets.

The abundance of volatiles is often considered as a factor in favor of habitability. Our results highlight the importance of considering their effect on global processes such as the thermal evolution of planets and magnetic field generation. Future studies should be conducted to decouple the role of redox state from volatile enrichment and describe how changing these parameters independently of one another changes radiogenic heating.

References

Barnes, R., Luger, R., Deitrick, R., Driscoll, P., Quinn, T. R., Fleming, D. P., Smotherman, H., McDonald, D. V., Wilhelm, C., Garcia, R., Barth, P., Guyer, B., Meadows, V. S., Bitz, C. M., Gupta, P., Domagal-Goldman, S. D., & Armstrong, J. (2020). VPLanet: The Virtual Planet Simulator. *Publications of the Astronomical Society of the Pacific*, *132*(1008), 024502. https://doi.org/10.1088/1538-3873/ab3ce8

Bedell, M., Bean, J. L., Meléndez, J., Spina, L., Ramírez, I., Asplund, M., Alves-Brito, A., Santos, L. dos, Dreizler, S., Yong, D., Monroe, T., & Casagrande, L. (2018). The chemical homogeneity of sun-like stars in the solar neighborhood. *The Astrophysical Journal*, *865*(1), 68. https://doi.org/10.3847/1538-4357/aad908

Boujibar, A., Driscoll, P., & Fei, Y. (2020). Super-Earth internal structures and initial thermal states. *Journal of Geophysical Research: Planets*, *125*(5). https://doi.org/10.1029/2019je006124

Boujibar, A., Righter, K., Bullock, E. S., Du, Z., & Fei, Y. (2020). Segregation of na, K, Rb and Cs into the cores of Earth, Mars and Vesta constrained with partitioning experiments. *Geochimica et Cosmochimica Acta*, *269*, 622–638. https://doi.org/10.1016/j.gca.2019.11.014

Boujibar, A., Andrault, D., Bolfan-Casanova, N., Bouhifd, M. A., & Monteux, J. (2015). Cosmochemical fractionation by collisional erosion during the Earth's accretion. *Nature Communications*, *6*(1). https://doi.org/10.1038/ncomms9295

Boujibar, A., Habermann, M., Righter, K., Ross, D. K., Pando, K., Righter, M., Chidester, B. A., & Danielson, L. R. (2019). U, th, and K partitioning between metal, silicate, and sulfide and implications for Mercury's structure, volatile content, and radioactive heat production. *American Mineralogist*, *104*(9), 1221–1237. https://doi.org/10.2138/am-2019-7000

Driscoll, P., & Olson, P. (2011). Optimal Dynamos in the cores of terrestrial exoplanets: Magnetic Field Generation and detectability. *Icarus*, *213*(1), 12–23. https://doi.org/10.1016/j.icarus.2011.02.010

Hemingway, D. J., & Driscoll, P. E. (2021). History and future of the martian dynamo and implications of a hypothetical solid inner core. *Journal of Geophysical Research: Planets*, *126*(4). https://doi.org/10.1029/2020je006663

Khan, A., Sossi, P. A., Liebske, C., Rivoldini, A., & Giardini, D. (2022). Geophysical and cosmochemical evidence for a volatile-rich Mars. *Earth and Planetary Science Letters*, *578*, 117330. https://doi.org/10.1016/j.epsl.2021.117330

Lay, T., Hernlund, J., & Buffett, B. A. (2008). Core–mantle boundary heat flow. *Nature Geoscience*, *1*(1), 25–32. https://doi.org/10.1038/ngeo.2007.44

Lodders, K. (2003). Solar system abundances and condensation temperatures of the elements. *The Astrophysical Journal*, *591*(2), 1220–1247. https://doi.org/10.1086/375492

Lugaro, M., Ott, U., & Kereszturi, Á. (2018). Radioactive nuclei from cosmochronology to habitability. *Progress in Particle and Nuclear Physics*, *102*, 1–47. https://doi.org/10.1016/j.ppnp.2018.05.002

McDonough, W. F., & Sun, S. -s. (1995). The composition of the Earth. *Chemical Geology*, *120*(3–4), 223–253. https://doi.org/10.1016/0009-2541(94)00140-4

Morard, G., Andrault, D., Antonangeli, D., & Bouchet, J. (2014). Properties of iron alloys under the Earth's core conditions. *Comptes Rendus Geoscience*, *346*(5–6), 130–139. https://doi.org/10.1016/j.crte.2014.04.007

Putirka, K. D., Dorn, C., Hinkel, N. R., & Unterborn, C. T. (2021). Compositional diversity of rocky exoplanets. *Elements*, *17*(4), 235–240. https://doi.org/10.2138/gselements.17.4.235

Unterborn, C. T., Johnson, J. A., & Panero, W. R. (2015). Thorium abundances in solar twins and analogs: Implications for the habitability of Extrasolar Planetary Systems. *The Astrophysical Journal*, *806*(1), 139. https://doi.org/10.1088/0004-637x/806/1/139

Wasson, J. T., & Kallemeyn, G. W. (1988). Compositions of chondrites. *Philosophical Transactions of the Royal Society of London. Series A, Mathematical and Physical Sciences*, *325*(1587), 535–544. https://doi.org/10.1098/rsta.1988.0066